NANO LETTERS

2007
Vol. 7, No. 10
2951−2959

Seeded Growth of Highly Luminescent CdSe/CdS Nanoheterostructures with Rod and Tetrapod Morphologies

Dmitri V. Talapin,*[,†,§] James H. Nelson,[‡] Elena V. Shevchenko,[†] Shaul Aloni,[†] Bryce Sadtler,[‡] and A. Paul Alivisatos[†,‡]

The Molecular Foundry, Lawrence Berkeley National Laboratory, Berkeley, California 94720, and Department of Chemistry, University of California, Berkeley, California 94720

Received August 10, 2007

ABSTRACT

We have demonstrated that seeded growth of nanocrystals offers a convenient way to design nanoheterostructures with complex shapes and morphologies by changing the crystalline structure of the seed. By using CdSe nanocrystals with wurtzite and zinc blende structure as seeds for growth of CdS nanorods, we synthesized CdSe/CdS heterostructure nanorods and nanotetrapods, respectively. Both of these structures showed excellent luminescent properties, combining high photoluminescence efficiency (~80 and ~50% for nanorods and nanotetrapods, correspondingly), giant extinction coefficients (~2×10^7 and ~1.5×10^8 M^{-1} cm^{-1} at 350 nm for nanorods and nanotetrapods, correspondingly), and efficient energy transfer from the CdS arms into the emitting CdSe core.

Colloidal synthesis of inorganic nanostructures is developing into a new branch of synthetic chemistry. Started with preparations of simple objects like spherical nanoparticles,[1,2] the field is now moving toward more and more sophisticated structures where size, shape, and connectivity of multiple parts of a multicomponent structure can be tailored in an independent and predictable manner.[3,4] Traditional molecular chemistry has proven that synthetic methodology should rely on a toolbox of robust and reproducible techniques. One of the major challenges in the colloidal synthesis of nanomaterials is balancing the two very different processes of nucleation and growth having different microscopic mechanisms, reaction orders, etc.[5,6] If the nanoparticle nucleation rate is not properly balanced with the growth rate, that is, the nucleation rate is either too slow or too fast with respect to the growth rate, the reaction will generate either bulk material or tiny clusters.[6,7] The conditions optimal for nucleating crystalline particles in a homogeneous solution might not be appropriate for tuning nanocrystal size and shape, and vice versa. Moreover, the nucleation stage can yield nuclei with unstable structure inducing phase transitions during nanoparticle growth.[8] For example, the synthesis of nanotetrapods is based on a delicate balance between stabilities of cubic and hexagonal phases in certain II−VI materials.[8,9] In a narrow window of reaction parameters, CdTe prefers nucleating in a zinc blende structure followed by the growth of four "arms" with a wurtzite structure.[8] Balancing all these processes in a one-pot reaction is difficult and leads to strong sensitivity on small variations in reaction conditions. Separation of nucleation and growth in colloidal synthesis can be achieved by adding preformed nuclei to the reaction mixture. Seeded growth has been successfully implemented in synthesis of core−shell and dumbbell nanocrystals.[10−12] In this letter, we demonstrate that both size and structure of the seeds can be used to design multicomponent nanostructures with complex shapes and peculiar optical properties.

Synthesis and properties of CdSe nanocrystals have been extensively investigated over the past two decades. Most classical preparative and spectroscopic studies have been carried out on CdSe nanocrystals with hexagonal (wurtzite) structure, further referred to as "w-CdSe". These can be obtained by reacting cadmium and selenium precursors in the presence of the stabilizing agents trioctylphosphine oxide (TOPO), trioctylphosphine (TOP), and hexadecylamine (HDA) at high temperatures, typically above 300 °C.[1,13] Recently CdSe nanocrystals with a cubic (zinc-blende) structure (further referred to as "zb-CdSe") have been synthesized by several groups.[14−16] In this work, we compared w-CdSe and zb-CdSe nanocrystals in the seeded growth of CdSe/CdS nanohererostructures with different morphologies. Combining CdSe and CdS in a single nanostructure creates a material with heterogeneous carrier

* Corresponding author. E-mail: dvtalapin@uchicago.edu.
† Lawrence Berkeley National Laboratory.
‡ University of California.
§ Current address: Department of Chemistry, The University of Chicago, Chicago, IL 60637.

10.1021/nl072003g CCC: $37.00 © 2007 American Chemical Society
Published on Web 09/11/2007

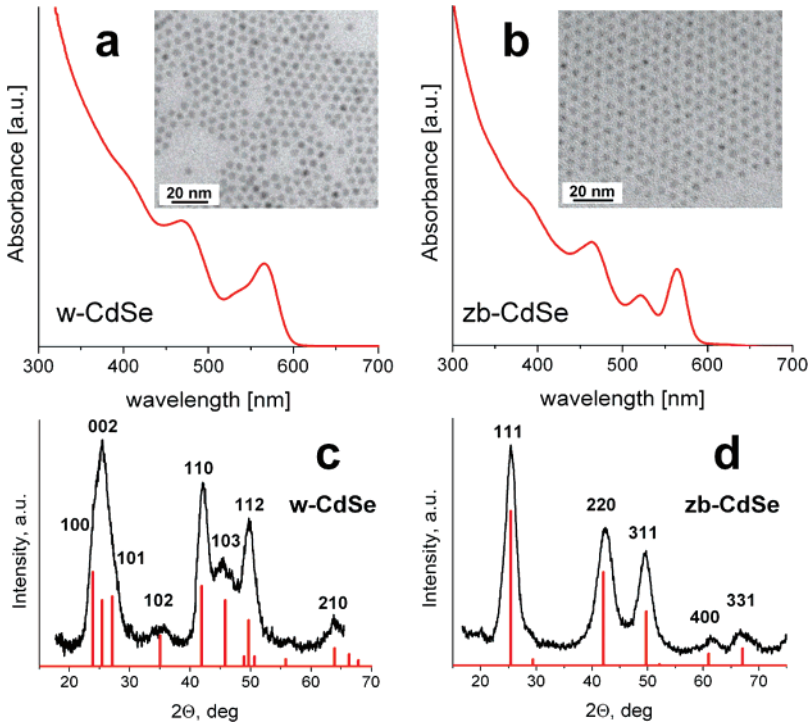

Figure 1. CdSe nanocrystals with wurtzite and zinc blende structures. (a) Absorption spectrum and TEM image of 4.4 nm CdSe nanocrystals with wurtzite lattice. (b) Absorption spectrum and TEM image of 4.0 nm CdSe nanocrystals with zinc blende lattice. (c,d) Powder X-ray (Cu K_α radiation) diffraction patterns of CdSe nanocrystals with wurtzite and zinc blende structures, correspondingly.

confinement or "mixed dimensionality" where holes are confined to CdSe while electrons can move freely between CdSe and CdS phases, spreading over the entire nanostructure.[11,17] Previously, we synthesized structures consisting of a spherical CdSe nanocrystal connected to a CdS nanorod.[17] In this structure, hole is three-dimensionally confined, whereas electron is confined only in two dimensions. Previously synthesized CdSe/CdS nanorods exhibited excellent luminescent properties with room-temperature photoluminescence quantum efficiencies (PL QE) above 50% and linearly polarized emission. The CdS nanorod can behave as an efficient antenna, absorbing light and funneling the excited carriers into the CdSe core where they radiatively recombine.[17] The very large absorption cross-sections of CdSe/CdS nanorods have been utilized in single-particle luminescence studies[18−21] and LEDs with polarized emission.[22] In addition, CdSe/CdS nanostructures exhibit novel properties originating from the concept of "mixed dimensionality": universal correlation between the spectral line width and the position of the excitonic transition in the single particle spectral jitter,[18,19] giant Stark effect,[20,21] the possibility of manipulating radiative lifetimes by applying an external electric field (exciton storage),[23] etc. Development of CdSe/CdS heterostructures with different morphologies will provide new possibilities for wave function engineering and tailoring optical and optoelectronic properties of semiconductor nanostructures.

We synthesized zb-CdSe nanocrystals via a slightly modified recipe of Cao et al. by reacting cadmium myristate with elemental selenium dissolved in 1-octadecene.[15] zb-CdSe nanocrystals nucleated at 170 °C and grew at 240 °C in the presence of oleic acid and oleylamine as the capping ligands. The size of zb-CdSe nanocrystal seeds can be tuned by varying the duration of nanocrystal growth at 240 °C. w-CdSe nanocrystals capped with HDA, TOPO, TOP, and a small amount of *n*-octyl- or *n*-tetradecylphosphonic acid have been synthesized as described in ref 13. The detailed synthetic recipes are given in the Experimental Details Section. Both approaches provide nearly spherical CdSe nanocrystals with size distribution below 10% and sharp excitonic features in the absorption spectra (Figure 1a,b). Both w-CdSe and zb-CdSe nanocrystals form stable colloidal solutions in nonpolar solvents like hexane, toluene, and TOP and show narrow PL bands associated with the recombination of photoexcited carriers from $1S_h$ and $1S_e$ quantum-confined states. The PL QE of both w-CdSe and zb-CdSe nanocrystals strongly depends on passivation of the nanocrystal surface with organic ligands, varying between ~3 and ~30% depending on sample history, for example, the number of precipitation−redissolution steps applied to purify the nanocrystals from crude solution.

Powder X-ray diffraction patterns of w-CdSe and zb-CdSe nanocrystals are shown in Figure 1c,d. The diffraction pattern of w-CdSe nanocrystals shows (102) and (103) reflections at 35.1° and 45.8° 2Θ angles, respectively, characteristic of the wurtzite phase. XRD patterns of zb-CdSe nanocrystals do not show these reflections. Instead, zb-CdSe nanocrystals exhibit a peak at 60.9°, which is the (400) reflection of zb-CdSe phase (Figure 1d). The peak around 25° in the diffraction pattern of w-CdSe nanocrystals is a convolution of (100), (002) and (101) reflections and is, therefore, broader than the (110) and (112) reflections at 42° and 49.7°, respectively (Figure 1c). In case of zb-CdSe nanocrystals all diffraction peaks showed similar broadening (Figure 1d). In

agreement with previous studies, the (102) and (103) reflections in the XRD patterns of w-CdSe are attenuated because of the presence of stacking faults along the (002) direction, a typical phenomenon in wurtzite II−VI nanocrystals.[1] For additional verification of our structural assignment, we synthesized ~15 nm diameter zb-CdSe nanocrystals by additional injections of Cd and Se precursors at 240 °C. The XRD pattern of these large CdSe nanocrystals shows narrow diffraction peaks matching all bulk zb-CdSe reflections. Large CdSe nanocrystals grown at 300 °C in the presence of HDA, TOPO, and TOP show well-resolved reflections of w-CdSe phase.[13]

We injected w-CdSe and zb-CdSe nanocrystals into the reaction mixture containing TOPO, TOP, *n*-octadecylphosphonic acid (ODPA), *n*-propylphosphonic acid (PPA), a Cd-ODPA complex and trioctylphosphine sulfide (TOPS) in concentrations optimized for synthesis of high-quality wurtzite-phase CdS (further referred to as "w-CdS") nanorods with long (001) axes (Supporting Information, Figure S1).[24] Low reactivity of the sulfur precursor determines very slow nucleation and growth of the CdS phase even at high reaction temperatures (320 °C). Typically, the nucleation of CdS nanorods starts 2−4 min after the injection of TOPS into the hot reaction mixture due to the high activation barrier for homogeneous nucleation of the CdS phase under these experimental conditions. A solution of CdSe seeds in TOP can be added to the reaction mixture either together with TOPS or 30−60 s later, that is, during the induction period. CdS easily nucleates at the surface of CdSe seeds.[11,17] We found that the structure of the CdSe seeds determined the morphology of CdSe/CdS nanoheterostructures. w-CdSe nanocrystals seeded the formation of CdSe/CdS nanorods (Figure 2a−c) whereas zb-CdSe seeds initiated growth of CdSe/CdS nanotetrapods (Figure 2d−f). XRD patterns of CdSe/CdS nanorods and nanotetrapods show that CdS prefers growing in the wurtzite phase both from w-CdSe and zb-CdS seeds (Supporting Information, Figure S2). The phosphonic acids present in the reaction mixture selectively bind to the {100} type facets of w-CdS and w-CdSe,[25] slowing the nanocrystal growth along these directions and forcing w-CdS to grow along the *c*-axis. The w-CdS phase will primarily nucleate on "polar" {001} and {00$\bar{1}$} facets of w-CdSe seeds, which are structurally identical to fast growing {001} and {00$\bar{1}$} facets of w-CdS.[17] The small mismatch in lattice constants of CdSe and CdS (~3.8% for the {001} planes) is favorable for the epitaxial relation between the CdSe and CdS parts of the nanostructure, observed in high-resolution transmission electron microscopy (HRTEM) images (Figure 3a). Analytical scanning electron transmission microscopy (STEM) studies confirmed the presence of CdSe seeds inside CdSe/CdS nanorods. The seed was always shifted toward one end of the nanorod (Figure 3b,c) due to the higher reactivity and faster growth of the {00$\bar{1}$} facet compared to the {001} facet.[26] In long nanorods, we often observed an increase in diameter around the CdSe cores (Figure 2b,c), which enables us to compare growth rates for the {001} and {00$\bar{1}$} planes. The distribution of relative facet growth rates within an ensemble of growing nanorods was

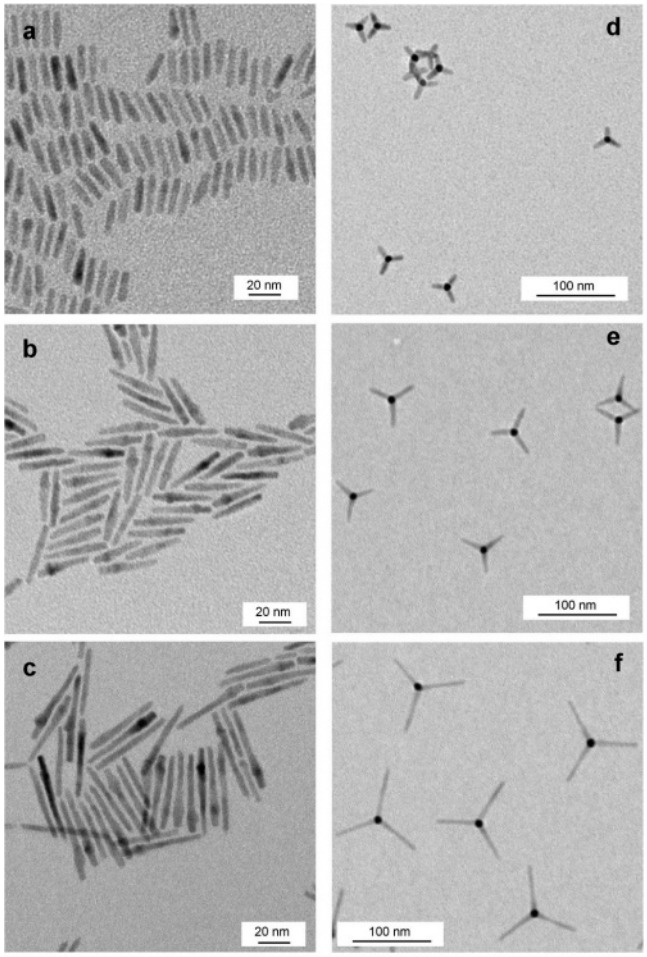

Figure 2. (a−c) TEM images of CdSe/CdS nanorods with different aspect ratios, all grown from 4.4 nm w-CdSe seeds. (d−f) TEM images of CdSe/CdS nanotetrapods with different lengths of the arms grown from 4.0 nm zb-CdSe seeds.

rather narrow and on the order of 10%. Typically, the {00$\bar{1}$} plane of CdS grew 2−3.5 times faster than the {001} plane. Tailoring the reaction conditions (concentration of w-CdSe seeds, growth time and concentration of sulfur precursor) allowed tuning the length of CdSe/CdS nanorods from 10 to ~63 nm, approaching an aspect ratio of ~13. The narrowest length and diameter distributions of the nanorods were observed at injection and growth temperatures of 340 and 320 °C, respectively. The narrow size distribution of the CdSe/CdS nanorods facilitated their self-assembly into superstructures with nematic and smectic ordering (Figure 4a and Supporting Information, Figure S3) as well as long-range ordered superlattices (Figure 4b,c). Addition of small amounts of HDA to a solution of CdSe/CdS nanorods in toluene assisted the growth of large superlattice domains with simple-hexagonal packing of nanorods oriented perpendicular to the substrate (Figure 4b,c and Supporting Information, Figure S3). Simple hexagonal packing can be stabilized by dipole−dipole interactions between the superlattice building blocks.[27]

Analytical STEM studies confirmed the presence of CdSe cores at the branch point of the nanotetrapods grown from zb-CdSe nanocrystals (Figure 5 and Supporting Information,

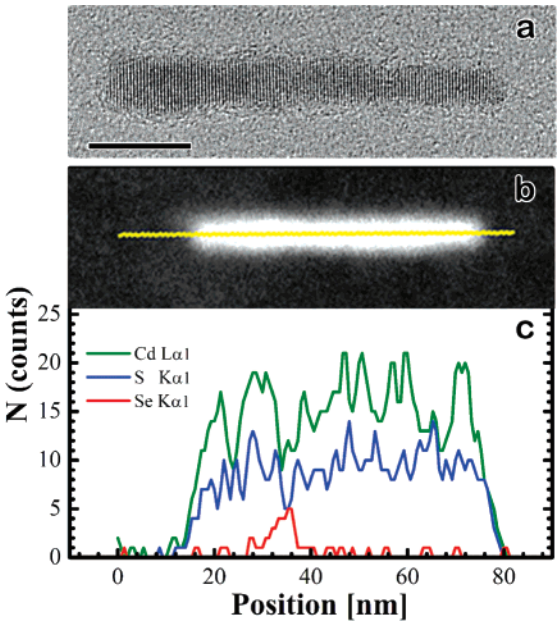

Figure 3. (a) HRTEM image of a CdSe/CdS nanorod grown from a 4.4 nm w-CdSe seed. Scale bar, 5 nm. (b) High-angle annular dark field (HAADF) image of a CdSe/CdS nanorod and (c) corresponding elemental profiles for Cd, S, and Se obtained by recording EDS signal intensities along the line shown in yellow in panel (b).

Figure S4). w-CdS nucleated on {111} facets of zb-CdSe nanocrystals that structurally match the fast-growing {001} planes of wurtzite lattice.[8,28] The atomic structure of an interface between the zb-core and the w-arms of CdSe/CdS nanotetrapod is shown in a HRTEM image of a tetrapod fragment (Figure 5b). HRTEM studies also revealed hexagonal faceting of CdS arms (Supporting Information, Figure S5). The length of the tetrapod arms can be tuned from ~5 up to ~50 nm by varying the concentration of CdSe seeds while keeping other reaction parameters constant. Lowering the concentration of CdSe seeds results in longer CdS arms. The length and thickness of the arms can be also controlled by adjusting the growth time, typically varied from 10 to 25 min, and the concentration of TOPS in the reaction mixture. Synthesis of CdSe/CdS nanotetrapods requires precise control of the reaction temperature because zb-CdSe seeds are metastable under the conditions of arm growth. Indeed, the synthesis of CdSe nanocrystals above 300 °C in the presence of TOPO, TOP, and ODPA yields pure w-CdSe phase. We found that high injection and growth temperatures (>340 °C) result in the formation of significant quantities of arrow-shaped nanorods, presumably because of partial transformation of zb-CdSe seeds into w-CdSe. To maximize the yield of nanotetrapods, we injected TOPS and zb-CdSe seeds at 290−300 °C slowly increasing the reaction temperature to 315 °C during the arm growth (~1°/min). To reduce the probability of seed phase transformation, we injected zb-CdSe seeds during the induction period, 40−60 s after the injection of TOPS. CdSe/CdS nanotetrapods can be isolated from the crude solution and reaction byproducts such as CdSe/CdS and CdS nanorods by standard precipitation−dissolution techniques described in the Experimental Details Section.

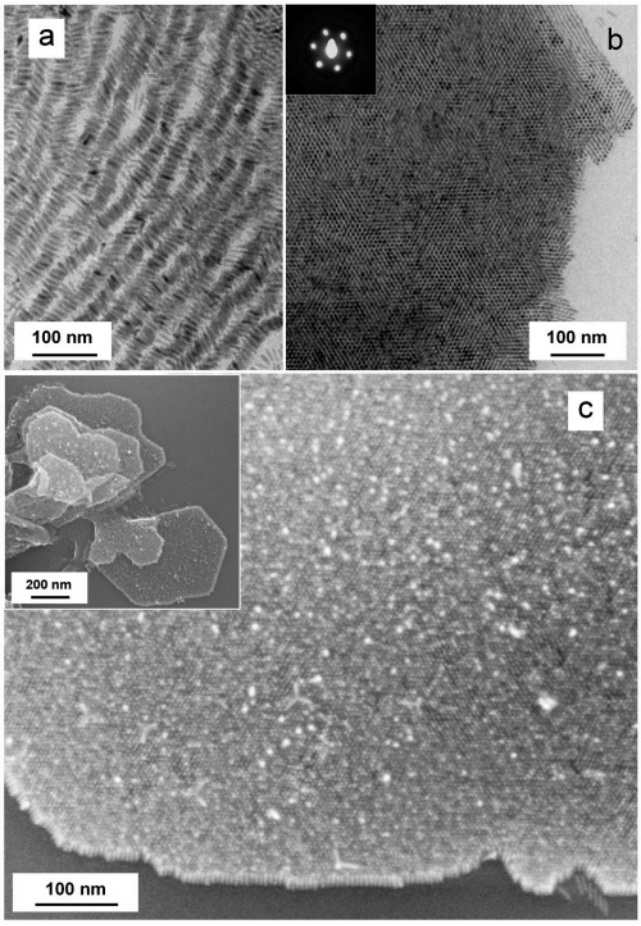

Figure 4. Self-assembly of CdSe/CdS nanorods with a length of 24 nm and a diameter of 5.2 nm. (a) TEM image of a superstructure with smectic-A ordering. (b) TEM image of a nanorod superlattice with simple hexagonal packing of nanorods assembled perpendicular to the substrate. Inset shows electron diffraction from a superlattice domain. (c) HRSEM image of CdSe/CdS nanorods assembled perpendicular to the substrate (silicon wafer). Inset shows layer-by-layer growth of a nanorod superlattice.

Both CdSe/CdS nanorods and nanotetrapods form stable and optically clear colloidal solutions in toluene, hexane, and other nonpolar organic solvents. The optical absorption spectra of CdSe/CdS nanorods and nanotetrapods, both grown from the CdSe seeds having the first excitonic transition at 563−565 nm show two characteristic features: the peaks in the red part of the spectrum, associated with the CdSe core, and very steep absorption onset below 500 nm, characteristic to the absorption by the CdS parts of the nanostructure (Figure 6a,b). Delocalization of the electron and hole wave functions into CdS results in a red shift of excitonic peaks in the CdSe/CdS heterostructures, thereby shifting the first excitonic maximum in absorption spectrum of 46 nm long, 4.4 nm diameter CdSe/CdS nanorods from 565 to 609 nm. In nanotetrapods with similar arm diameter, the red shift is significantly larger; the first excitonic peak shifts from 563 to 623 nm upon growth of 25 nm long CdS arms. Larger red shift in heterostructures with tetrapod morphology compared to nanorods can originate both from the intrinsic difference in energy levels of w-CdSe and zb-

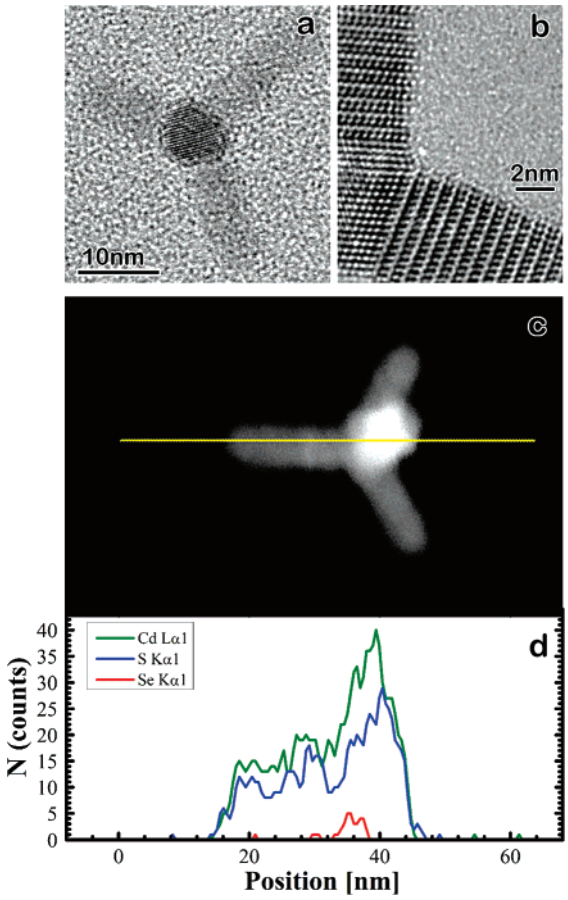

Figure 5. (a) TEM image of a CdSe/CdS nanotetrapod grown from the 4 nm zb-CdSe seed. (b) HRTEM image of a tetrapod fragment showing the interface between {111} planes of zb-CdSe seed and {001} planes of w-CdS arms. (c) High angle annular dark field (HAADF) image of a CdSe/CdS nanotetrapod and (d) corresponding elemental profiles for Cd, S, and Se obtained by recording energy-dispersive X-ray intensities (EDS) along the line shown in yellow in panel (c). Two-dimensional elemental map of a CdSe/CdS nanotetrapod is shown in Supporting Information, Figure S4.

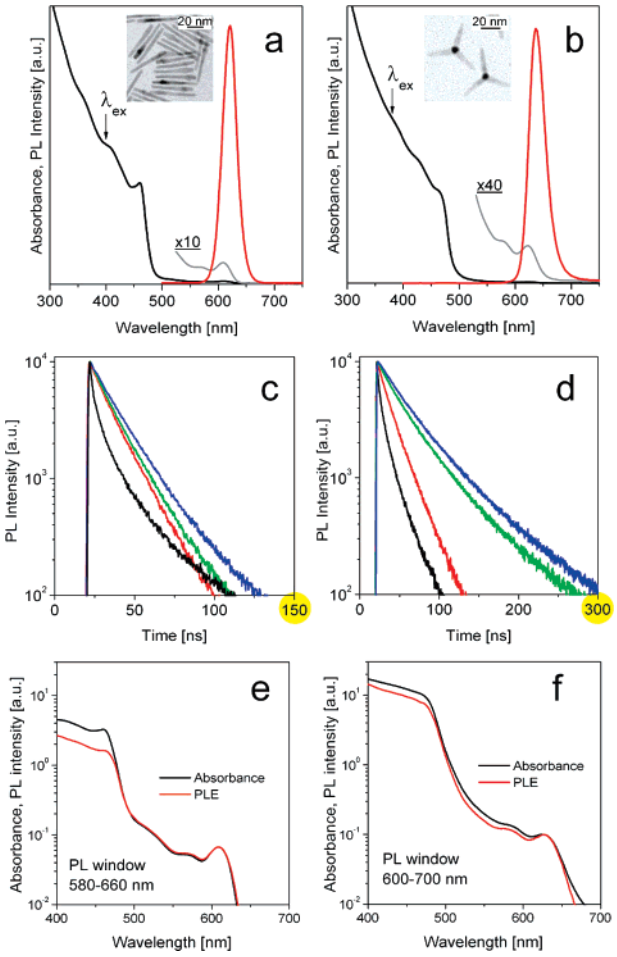

Figure 6. **(a)** Absorption (black) and PL (red) spectra of toluene solutions of 46 nm long CdSe/CdS nanorods grown from 4.4 nm w-CdSe seeds. Gray line shows magnified absorption spectrum to emphasize the structure of the absorption onset. Absolute PL quantum efficiency of this sample was 80%, measured at the excitation wavelength 514 nm. **(b)** Absorption (black) and PL (red) spectra of toluene solutions of CdSe/CdS nanotetrapods with 24 nm CdS legs grown from 4 nm zb-CdSe seeds. Gray line shows magnified absorption spectrum to emphasize structure of the absorption onset. Absolute PL quantum efficiency of this sample was 39%, measured at the excitation wavelength 512 nm. **(c)** Fluorescence decay of 4.4 nm w-CdSe nanocrystals (black) and CdSe/CdS nanorods with different lengths: 12.2 nm (red), 24 nm (green), and 36 nm (blue). All samples were excited at 440 nm; emission was detected at the maxima of the PL spectra. **(d)** Fluorescence decay of 4.0 nm zb-CdSe nanocrystals (black) and CdSe/CdS nanotetrapods with arm length of 9.2 nm (red), 24 nm (green), and 38 nm (blue). All samples were excited at 440 nm; emission was detected at the maxima of the PL spectra. **(e)** Comparison of absorption and PL excitation spectra for 46 nm CdSe/CdS nanorods shown in panel (a). PL intensity was integrated throughout the entire emission band. Absorbance in the first excitonic maximum was normalized to 0.1. **(f)** Comparison of absorption and PL excitation spectra for CdSe/CdS nanotetrapods with 24 nm long CdS arms shown in panel (b). PL intensity was integrated throughout the entire emission band. Absorbance in the first excitonic maximum was normalized to 0.1.

CdSe seeds and shape effects on electronic states in these nanostructures.[31]

Below 500 nm, CdS provides the major contribution to the absorption of our CdSe/CdS nanostructures. The dominance of the arm absorption is most pronounced in the case of nanotetrapods where the absorption of the CdSe cores can barely be seen without zooming in to the red part of the absorption spectrum (Figure 6b). In nanotetrapods with 50 nm long arms, the absorption cross section of the CdS arms is ~300 times larger than the absorption cross section of the CdSe core (Supporting Information, Figure S6), implying that more than 99% of the incident light is absorbed by the arms of the tetrapod. The CdSe-related absorption peaks can be used as an internal standard to calculate the molar extinction coefficient (ϵ) of CdSe/CdS nanorods and nanotetrapods. Our earlier studies revealed that the oscillator strength of the first excitonic transition in CdSe/CdS nanorods is comparable to that of bare CdSe cores.[17,30] The 4.4 nm w-CdSe nanocrystals have $\epsilon \sim 2.5 \times 10^5$ M^{-1} cm^{-1} at the first absorption maximum.[31] We obtained similar values (±30%) for ϵ of bare zb-CdSe nanocrystals. Thus, 46 nm long CdSe/CdS rods have $\epsilon \sim 2 \times 10^7$ M^{-1} cm^{-1} at 350 nm and $\epsilon \sim 4 \times 10^7$ M^{-1} cm^{-1} at 300 nm. These impressive values look small when compared to extinction coefficients of the nanotetrapods, which have ϵ above 10^8 M^{-1} cm^{-1}!

Our estimates for a solution of tetrapods with ~50 nm long CdS arms give $\epsilon \sim 1.5 \times 10^8$ M^{-1} cm^{-1} at 350 nm and $\epsilon \sim 3 \times 10^8$ M^{-1} cm^{-1} at 300 nm. The absorption cross section of individual arms of a tetrapod (e.g., CdS nanorods) should be strongly dependent on their orientations with respect to polarization of incoming photons. However, four CdS nanorods arranged around a CdSe core in the form of tetrapod arms form a perfect antenna that effectively captures photons coming from any direction and with any polarization, leading to a giant absorption cross section of the entire construction.

CdSe/CdS nanorods and nanotetrapods exhibit luminescence with high quantum yield. They can emit in the yellow, orange, or red part of the spectrum, depending on the size of the CdSe seed and diameter of the CdS rods, whereas the length of the nanorod or tetrapod arms has a minor effect on the emission wavelength. Spectral position of the emission band shows that the radiative recombination of photoexcited carriers occurs in the CdSe core, whereas the emission of CdS arms is strongly suppressed (Figure 6a,b). The global Stokes shift observed for our CdSe/CdS nanorods is ~41−46 meV, nearly independent of the nanorod length,[32] whereas the Stokes shift in nanotetrapods is larger, approaching ~78 meV, and rises with increasing length of the CdS arms. The room-temperature PL quantum efficiencies of the CdSe/CdS nanorods were typically 75−80%. The error of our PL QE measurements was found to be ≤10% and has been verified by using a series of laser dyes emitting in different parts of the spectrum (Rhodamine 6G, Rhodamine 640, LD 690) and measuring their PL efficiencies with respect to each other. In contrast to bare CdSe nanocrystals whose PL QE is strongly dependent on sample history, washing the nanorods from the crude solution by several precipitation/redissolution steps did not result in significant drops in the PL efficiency. We routinely observed PL QEs above 75% after two purification stages. Time-resolved PL measurements show nearly linear fluorescence decays (Figure 6c), characteristic of a single dominant recombination channel and a reduced role of trapping-detrapping processes at the nanorod surface. The radiative decay rate gradually decreased with increasing nanorod length (Figure 6c), as expected because of the reduced oscillator strength due to the decreased electron−hole wave function overlap.[20] Bare w-CdSe seeds show fast nonlinear decay because of the presence of nonradiative recombination channels.

The PL QEs of CdSe/CdS nanotetrapods were typically between 35 and 60%. Generally, the samples with skinnier arms exhibited higher PL efficiencies compared to the tetrapods with "fat" arms, while the length of the arms had a minor effect on the PL QE. CdSe/CdS nanotetrapods showed significantly larger PL lifetimes compared to CdSe/CdS nanorods with similar arm diameter (Figure 6d). To understand this result, the photophysics of zb-CdSe nanocrystals has to be studied. To the best of our knowledge, there were no experimental studies of the electronic structure and the emitting state in the zb-CdSe nanocrystals. Our preliminary results show ~25% lower radiative rates for zb-CdSe nanocrystals compared to w-CdSe ones, estimated as $\tau_{rad}^{-1} = (\text{PL QE})/\tau_{PL}$, where τ_{PL} is approximated as 1/e of the PL decay time. Additionally, the crystal field can induce large perturbations to the electronic structure in nanocrystals with significant shape anisotropy. Semiempirical pseudopotential calculations by Li and Wang showed that the lowest electronic state in a nanocrystal with tetrapod morphology is completely localized in the central tetrahedron while the first hole state is more delocalized and is present in the arms of the tetrapod.[29] In CdSe/CdS tetrapod heterostructures where the hole is localized in CdSe by the valence band offset, we should expect localization of both electron and hole states in the center of the tetrapod, maximizing the wave function overlap and leading to high luminescence efficiency. Quantum confinement in narrow-arm tetrapods should result in a higher degree of localization of the electron wave function at the branch point. In accord with this prediction, we observed an increase of the radiative rate in tetrapods with decreasing arm diameter.

CdSe/CdS nanorods and tetrapods have giant absorption cross sections below 500 nm due to the efficient light absorption by the CdS arms. Our earlier studies demonstrated very efficient charge transfer from the CdS rod to the emitting CdSe core.[17] To quantify the efficiency of transfer from CdS to CdSe in heterostructures with different morphologies, we measured PL excitation (PLE) spectra. We observed quantitative agreement between absorption and PLE spectra for short (<20 nm) CdSe/CdS nanorods demonstrating that all electron−hole pairs generated in CdS are captured by the w-CdSe core. In the case of long (46 nm) rods, some portion of the photoexcited carriers recombine in the CdS arms, as evidenced from the difference between absorption and PLE spectra below 465 nm (Figure 6e) and the appearance of a very weak emission band around 470 nm. In the case of nanotetrapods with similar absorption cross section, the exciton travel path from the CdS arms into the emitting zb-CdSe core is about four times shorter, resulting in more efficient carrier collection. Indeed, we observed nearly quantitative agreement between absorption and PLE spectra of the nanotetrapods with 24 nm long arms (Figure 6f). The combination of a giant absorption cross section and efficient energy transfer from CdS arms into the highly emitting CdSe core places CdSe/CdS nanotetrapods among the best light harvesting systems and makes it particularly useful for various applications such as light concentrators, solar cells, and LEDs. Four CdS arms of a tetrapod can be used for pumping carriers into the CdSe core, leading to lower lasing thresholds. Further interesting results are likely to come from spectroscopic studies of single CdSe/CdS nanotetrapods that are currently underway.

In summary, we have demonstrated an efficient way of engineering the shape of nanocrystal heterostructures by tailoring the phase of the nanocrystal seeds. These results should be considered as a significant step on the way toward controllable synthesis of complex multicomponent nanostructures with precisely designed physical and chemical properties.

Experimental Details. *Wurtzite CdSe Nanocrystals.* 10.0 g (25.9 mmol) of TOPO and 5.00 g (20.7 mmol) of HDA were loaded into a 50 mL three-neck flask and heated to

110 °C for 50 min under vacuum. Under the flow of N_2, either 0.400 g (1.52 mmol) of TDPA or 0.300 g (1.68 mmol) of OPA was quickly added, and the reaction was degassed under vacuum for another 5 min. Reaction mixtures with TDPA produced smaller nanoparticles, whereas mixtures with OPA allowed for growth of particles with diameters above 4.5 nm. The reaction mixture was heated to 300 °C under flowing N_2, and an injection solution of 1 mmol TOPSe and 1.64 mmol dimethylcadmium dissolved in 5 mL of TOP was rapidly injected into the stirring mixture. Additional injections of stock solution to reactions containing OPA were necessary to grow particles larger than 5 nm. Reactions were kept at 300 °C under flowing N_2 overnight at which time they were cooled to room temperature and opened to air. The resulting solid was transferred into the glovebox and dissolved in anhydrous toluene. The vial was centerfuged to remove any solids, and the subsequent mixture was precipitated with anhydrous ethanol and resuspended in anhydrous toluene.

Zinc Blende CdSe Nanocrystals. In a 100 mL three-neck flask, 0.34 g (0.6 mmol) of cadmium myristate was dissolved in 37 mL of 1-octadecene and degassed upon heating at 90 °C under vacuum for 40 min. The solution was cooled to room temperature, and 0.024 g (0.3 mmol) of 100 mesh Se powder (99.999%) was added to the reaction mixture, followed by degassing at 50 °C under vacuum for 10 min. The reaction mixture was heated to 240 °C (∼24 deg/min) under N_2 atmosphere. zb-CdSe nanocrystals nucleated at ∼170 °C, observed through the change of the solution color from colorless to yellow. The reaction temperature was allowed to rise up to 240 °C. A degassed solution of 0.1 mL of oleic acid and 1 mL of oleylamine in 4 mL of 1-octadecene was added dropwise to the reaction mixture ∼3 min after approaching 240 °C to stabilize the nanoparticle growth. The growth of nanocrystals can be visually monitored by the change of solution color from yellow to deep red and by taking aliquots for UV−vis and PL measurements. Typically, it took zb-CdSe nanocrystals ∼2 h to grow from initial nuclei to 5 nm diameter nanocrystals. Larger nanocrystals can be synthesized by additional injections of Cd and Se precursors to the reaction mixture at 240 °C. After cooling the reaction mixture to room temperature, zb-CdSe nanocrystals were precipitated by adding ethanol or acetone to the crude solution, transferred to a glovebox and redispersed in anhydrous hexane. The purification step can be repeated several times by using different solvent/nonsolvent combinations.

Cadmium myristate can be synthesized as described in ref 15 or prepared in situ by reacting 0.077 mg of CdO with 0.29 g of myristic acid in 5 mL of 1-octadecene at 250 °C followed by the addition of 32 mL of 1-octadecene and then degassing the solution at 80 °C under vacuum for 1 h.

Preparation of Stock Solutions of w-CdSe and zb-CdSe seeds. The concentration of w-CdSe nanocrystals was calculated using the size dependent molar extinction coefficient given in refs 31,33. Particle size was determined by the position of the first exciton peak maximum. We used the sizing curve published in the Supporting Information to ref 34.

We could not find information about the size dependent molar extinction coefficients for zb-CdSe nanocrystals. To calculate the concentration of our zb-CdSe seed solutions, we thoroughly purified colloidal solutions of zb-CdSe nanocrystals by 5−6 precipitation/redissolution steps under inert atmosphere using different combinations of anhydrous solvents and nonsolvents (hexane/acetone, hexane/ethanol, toluene/methanol, toluene/acetonitrile, chloroform/methanol, chloroform/acetone, etc.) to purify the nanocrystals from any residual precursors and high-boiling solvents. Then, zb-CdSe nanocrystals were dissolved in anhydrous hexane and filtered through a 0.2 μm PTFE filter. We measured the weight of the nanocrystals after evaporating hexane and correlated it with the absorbance of the nanocrystals. This procedure allowed us to estimate the molar extinction coefficient of zb-CdSe nanocrystals, which was found to be similar to that of w-CdSe nanocrystals within the ∼30% error introduced by the surface ligands.

Solutions for Synthesis of CdSe/CdS Nanorods and Nanotetrapods. 0.207 g (1.61 mmol) of CdO, 1.08 g (3.23 mmol) of *n*-octadecylphosphonic acid (Polycarbon, 99%), 0.015 g (0.12 mmol) of *n*-propylphosphonic acid, and 3.35 g (9.18 mmol) of TOPO (Aldrich Reagent Plus, 99%) were loaded into a 25 mL three-neck flask and heated to 120 °C for 30 min under vacuum. The mixture was heated to 320 °C under flowing N_2 to produce an optically clear solution. After the CdO completely dissolved, the solution was cooled to 120 °C and put under vacuum for 2 h, after which it was heated to 340 °C (for nanorod synthesis) or 300 °C (for nanotetrapod synthesis) under flowing N_2. At this time, 1.5 g (4.05 mmol) of TOP (Strem, 97%) was injected and the flask was allowed to return to 340 °C (for nanorod synthesis) or 300 °C (for nanotetrapod synthesis).

TOPS was prepared by reacting equimolar amounts of TOP and elemental sulfur at 50 °C under inert atmosphere.

Synthesis of CdS/CdSe Rods. 0.65 g TOPS (1.61 mmol) was injected into the Cd/ODPA/PPA/TOPO/TOP solution at 340 °C, followed after 20 s by the injection of $\sim 10^{-8}$ mol of w-CdSe seeds (∼2 mg of CdSe in the case of 4.4 nm nanocrystals) dissolved in 0.50 g (1.35 mmol) of TOP. The w-CdSe solution was prepared by concentrating 1 mL of 10^{-5} M solution of w-CdSe nanocrystals in toluene under vacuum to ∼0.05 mL and adding 0.5 g of TOP (gentle sonication might be necessary to disperse the CdSe nanocrystals in TOP). The reaction temperature was adjusted to 320 °C, and after 10 min the reaction was stopped by the injection of 10 mL of anhydrous toluene and the removal of the heating mantle. Once the flask reached room-temperature, it was opened to air. CdSe/CdS nanorods were isolated by mixing the crude solution with toluene (∼1:1 by volume) and adding ethanol to induce flocculation followed by centrifugation to precipitate the nanorods. Precipitated nanorods were redispersed in hexane/octylamine (8:1 by volume) mixture and precipitated again with ethanol. The resulting

CdS/CdSe nanorods formed stable colloidal solutions in toluene and exhibited bright and stable luminescence in air for months.

The above recipe produced 46 ± 9 nm rods with a small bump on one side indicating the position of the CdSe dot inside the rod. The diameter of these rods as measured at the center of the rod's length was 4.2 ± 0.5 nm. Modifications to this synthetic procedure allow for control of nanorod length and diameter. The diameter and length of the rods could be controlled by the amount of TOPS injected into the reaction; more TOPS produces longer and skinnier rods. Using 0.330 g of TOPS gives 24 ± 2 nm long rods with a diameter of 5.2 ± 0.5 nm, and 1.30 g of TOPS yields 55 ± 12 nm long rods with a diameter of 4.2 ± 0.5 nm. Also, the length of the rods could be controlled by the injection of different amounts of CdSe dots with more dots producing shorter rods. A sample of 3.0×10^{-8} mol of dots gives rods a length of 22 ± 4 nm and a diameter of 5.2 ± 0.7 nm. Finally, the reaction time could be changed to control rod length; longer growth times produce longer rods with a 3 min growth giving 12 ± 1 nm long rods with a diameter of 4.7 ± 0.5 nm.

CdS/CdSe Tetrapods. 0.65 g of TOPS was injected into the Cd/ODPA/PPA/TOPO/TOP solution at 300 °C, followed after 40 s by the injection of zb-CdSe seeds (2 mg of zb-CdSe nanocrystals, $\sim 10^{-8}$ mol of 4.0 nm nanocrystals) dissolved in 0.50 g of TOP. The zb-CdSe solution was prepared by mixing 0.5 mL of 4 mg/mL solution of 4.0 nm zb-CdSe nanocrystals in hexane with 0.5 g of TOP followed by evaporating the hexane under vacuum. The reaction temperature was increased to 315 °C (~1 deg/min). The growth of the CdS arm continued for 15−25 min and was stopped by cooling the reaction mixture to room temperature. The length of tetrapod arms was varied by adjusting the concentration of zb-CdSe seeds. Thus, 6, 4, 2, and 1 mg of 4.0 nm zb-CdSe seeds yielded CdSe/CdS nanotetrapods with arm lengths of 15, 19, 24, and 46 nm, correspondingly. Longer growth times typically resulted in increasing the diameter of CdS arms. As-synthesized CdSe/CdS nanotetrapods can be isolated by adding toluene to the crude solution and flocculating the tetrapods with acetone. The precipitate was redispersed in hexane/octylamine (8:1 by volume) mixture and precipitated with acetone (~8:6 hexane-to-acetone ratio). The collected precipitate can be redispersed in toluene or hexane. Often the as-synthesized nanotetrapods contain some impurities such as CdSe/CdS and CdS nanorods. These can be separated from nanotetrapods by size- and shape-selective precipitation. We centrifuged solutions of tetrapods in toluene at 12000 × G for 15 min. Because the tetrapods are significantly heavier than the nanorods, they concentrated at the bottom of centrifugation tube. The supernatant was carefully removed, and the concentrated tetrapod solution was diluted with toluene. Repeating this procedure twice allowed us to remove the nanorods and other reaction byproducts.

Acknowledgment. We thank S. Claridge and P. Guyot-Sionnest for stimulating discussions and T. Mattox for technical support. Work at the Molecular Foundry was supported by the Director, Office of Science, Office of Basic Energy Sciences, Division of Materials Sciences and Engineering, of the U.S. Department of Energy under Contract DE-AC02-05CH11231.

Supporting Information Available: TEM images of CdS nanorods grown in the absence of CdSe seeds (Figure S1); X-ray diffraction patterns of CdSe/CdS nanorods and nanotetrapods (Figure S2); TEM images of CdSe/CdS nanorods self-assembled into a superstructure with nematic and crystalline ordering (Figure S3); two-dimensional elemental map for a nanotetrapod obtained from analytical TEM (Figure S4); HRTEM of a CdSe/CdS nanotetrapod (Figure S5); absorption and PL spectra of CdSe/CdS nanotetrapods with 50 nm long arms (Figure S6).

References

(1) Murray, C. B.; Norris, D. J.; Bawendi, M. G. *J. Am. Chem. Soc.* **1993**, *115*, 8706.
(2) Brust, M.; Walker, M.; Bethell, D.; Schiffrin, D. J.; Whyman, R. J. *Chem. Commun.* **1994**, 801.
(3) Milliron, D. J.; Hughes, S. M.; Cui, Y.; Manna, L.; Li, J.; Wang, L.-W.; Alivisatos, A. P. *Nature* **2004**, *430*, 190.
(4) Cozzoli, P. D.; Pellegrino, T.; Manna, L. *Chem. Soc. Rev.* **2006**, *35*, 1195.
(5) Sugimoto, T. *Adv. Colloid Interface Sci.* **1987**, *28*, 65.
(6) Shevchenko, E. V.; Talapin, D. V.; Schnablegger, H.; Kornowski, A.; Festin, O.; Svedlindh, P.; Haase, M.; Weller, H. *J. Am. Chem. Soc.* **2003**, *125*, 9090.
(7) Yu, W. W.; Peng, X. *Angew. Chem., Int. Ed.* **2002**, *41*, 2368.
(8) Manna, L.; Milliron, D.; Meisel, A.; Scher, E. C.; Alivisatos, A. P. *Nat. Mater.* **2003**, *2*, 382.
(9) Carbone, L.; Kudera, S.; Carlino, E.; Parak, W. J.; Giannini, C.; Cingolani, R.; Manna, L. *J. Am. Chem. Soc.* **2006**, *128*, 748.
(10) Hines, M. A.; Guyot-Sionnest, P. *J. Phys. Chem.* **1996**, *100*, 468.
(11) Peng, X.; Schlamp, M. C.; Kadavanich, A.; Alivisatos, A. P. *J. Am. Chem. Soc.* **1997**, *119*, 7019.
(12) Yu, H.; Chen, M.; Rice, P. M.; Wang, S. X.; White, R. L.; Sun, S. *Nano Lett.* **2005**, *5*, 379.
(13) Talapin, D. V.; Rogach, A. L.; Kornowski, A.; Haase, M.; Weller, H. *Nano Lett.* **2001**, *1*, 207.
(14) Rogach, A. L.; Kornowski, A.; Gao, M.; Eychmuller, A.; Weller, H. *J. Phys. Chem. B* **1999**, *103*, 3065.
(15) Yang, Y. A.; Wu, H.; Williams, K. R.; Cao, Y. C. *Angew. Chem., Int. Ed.* **2005**, *44*, 6712.
(16) Han, L.; Qin, D.; Jiang, X.; Liu, Y.; Wang, L.; Chen, J.; Cao, Y. *Nanotechnology* **2006**, *17*, 4736.
(17) Talapin, D. V.; Koeppe, R.; Götzinger, S.; Kornowski, A.; Lupton, J. M.; Rogach, A. L.; Benson, O.; Feldmann, J.; Weller, H. *Nano Lett.* **2003**, *3*, 1677.
(18) Müller, J.; Lupton, J. M.; Rogach, A. L.; Feldmann, J.; Talapin, D. V.; Weller, H. *Phys. Rev. Lett.* **2004**, *93*, 167402.
(19) Müller, J.; Lupton, J. M.; Rogach, A. L.; Feldmann, J.; Talapin, D. V.; Weller, H. *Phys. Rev. B* **2005**, *72*, 205339.
(20) Muller, J.; Lupton, J. M.; Lagoudakis, P. G.; Schindler, F.; Koeppe, R.; Rogach, A. L.; Feldmann, J.; Talapin, D. V.; Weller, H. *Nano Lett.* **2005**, 5, 2044.
(21) Becker, K.; Lupton, J. M.; Müller, J.; Rogach, A. L.; Talapin, D. V.; Weller, H.; Feldmann, J. *Nat. Mater.* **2006**, *5*, 777.
(22) Hikmet, R. A. M.; Chin, P. T. K.; Talapin, D. V.; Weller, H. *Adv. Mater.* **2005**, *17*, 1436.
(23) Kraus, R. M.; Lagoudakis, P. G.; Rogach, A. L.; Talapin, D. V.; Weller, H.; Lupton, J. M.; Feldmann, J. *Phys Rev. Lett.* **2007**, *98*, 017401.
(24) Robinson, R. D.; Sadtler, B.; Demchenko, D. O.; Erdonmez, C. K.; Wang, L.-W.; Alivisatos, A. P. *Science* **2007**, *317*, 355.
(25) Li, J.; Wang, L.-W. *Nano Lett.* **2003**, *3*, 1357.
(26) Manna, L.; Scher, E. C.; Alivisatos, A. P. *J. Am. Chem. Soc.* **2000**, *122*, 12700.
(27) Talapin, D. V.; Shevchenko, E. V.; Murray, C. B.; Titov, A. V.; Kral, P. *Nano Lett.* **2007**, *7*, 1213.
(28) Xie, R.; Kolb, U.; Basche, T. *Small* **2006**, *2*, 1454.

(29) Manna, L.; Wang, L. W.; Cingolani, R.; Alivisatos, A. P. *J. Phys. Chem. B* **2005**, *109*, 6183.
(30) Talapin, D. V.; Shevchenko, E. V.; Murray, C. B.; Kornowski, A.; Forster, S.; Weller, H. *J. Am. Chem. Soc.* **2004**, *126*, 12984 and Supporting Information.
(31) Yu, W. W.; Qu, L.; Guo, W.; Peng, X. *Chem. Mater.* **2003**, *15*, 2854.
(32) This observation appears to disagree with our results obtained on shorter CdSe/CdS nanorods synthesized at 120 °C using HDA and TOPO as the capping ligands[17]. The inconsistency could originate from a structural difference between CdSe/CdS nanorods synthesized at 320 °C and capped with ODPA and those grown at 120 °C in the presence of HDA: at 320 °C CdS nucleates and grows both on {001} and $\{00\bar{1}\}$ facets of the w-CdS seed, whereas at 120 °C we observed the growth of the CdS rod solely from the $\{00\bar{1}\}$ facet. Moreover, at 320 °C partial alloying of CdSe and CdS phases can take place.
(33) Leatherdale, C. A.; Woo, W.-K.; Mikulec, F. V.; Bawendi, M. G. *J. Phys. Chem. B* **2002**, *106*, 7619.
(34) Mikulec, F. V.; Kuno, M.; Bennati, M.; Hall, D. A.; Griffin, R. G.; Bawendi, M. G. *J. Am. Chem. Soc.* **2000**, *122*, 2532.

NL072003G